ELSEVIER

Biophysical Chemistry 55 (1995) 215–230

Biophysical Chemistry

Structural features of isolated M2 helices of nicotinic receptors. Simulated annealing via molecular dynamics studies

R. Sankararamakrishnan, M.S.P. Sansom *

Laboratory of Molecular Biophysics, The Rex Richards Building, University of Oxford, South Parks Road, Oxford, OX1 3QU, UK

Received 19 August 1994; revised 11 January 1995; accepted 12 January 1995

Abstract

The nicotinic acetylcholine receptor is an integral membrane protein and a ligand-gated cation channel. It has stoichiometry $\alpha_2\beta\gamma\delta$, the subunits arranged symmetrically around an approximate five-fold axis. Five M2 helices, one from each subunit, form a parallel helix bundle surrounding a central pore. Simulated annealing via restrained molecular dynamics (SA/MD) has been employed to generate ensembles of isolated M2 transmembrane helices. Four ensembles of two different M2 helix sequences, M2δ and M2γ, have been generated by SA/MD. The ensembles differed in their treatment of electrostatic interactions. Analysis of the simulated structures showed that intra-helical H-bonds were more strongly conserved in the C-terminal (and more hydrophobic) segment of M2 helices. Conformations of polar sidechains have been analyzed, placing particular emphasis on EK (and QK) pairs at the N-termini of M2δ (and M2γ) helices. Conformations of EK sidechain pairs were obtained for the high resolution structures in the protein database in order to guide our analysis of simulated structures. Serine and threonine sidechain conformations in the M2 models also have been determined. Implications of studies of isolated M2 helices for models of the intact pore region of the nicotinic receptor are discussed.

Keywords: Ion channel; Transmembrane helice; Molecular dynamics; Electrostatics; Salt-bridge; Sidechain conformation

1. Introduction

There has been considerable progress in unravelling the principles of membrane protein structure over the past decade. Experimentally determined structures are known for several integral membrane proteins formed by bundles of transmembrane (TM) α-helices, and more such structures will be solved at high resolution in the near future. Furthermore, there is now a good understanding of how TM helices assemble within lipid bilayers. Considerable evidence suggests that isolated TM helices form independent folding domains [1]. In particular, studies on synthetic single TM helices from bacteriorhodopsin [2,3] and on α-helical channel-forming peptides [4] support this theory.

One isolated TM helix which has been the subject of several investigations is the M2 helix of the nicotinic acetylcholine receptor (nAChR). The nAChR is a cation-selective ion channel which mediates signal transmission at chemical synapses (for a recent review see [5]). The nAChR is a pentamer, with stoichiometry $\alpha_2\beta\gamma\delta$, the four subunit types showing strong sequence similarities. Cryoelectron

* Corresponding author.

SSDI 0301-4622(95)00006-2

microscopy studies reveal that the intact receptor has approximate five-fold symmetry, the symmetry axis coinciding with the central transbilayer pore [6]. Hydrophobicity analysis suggested the presence of four hydrophobic regions (M1 to M4) within the nAChR sequence. On the basis of 9 Å resolution structural studies [7], chemical labelling experiments [8,9], and site-directed mutagenesis studies [10–13] it is believed that five M2 helices, one from each subunit, form a bundle of approximately parallel helices surrounding a central pore [14]. A synthetic peptide corresponding to M2δ from *Torpedo* nAChR has been shown to self-assemble within planar lipid bilayers to form channels with conductance properties similar to those of the intact protein [15]. Circular dichroism studies [16] and solid state NMR experiments [17] suggest that M2δ adopts an α-helical conformation when in a membrane mimetic environment. On this basis, it is of interest to study the structural features of isolated M2 helices, which in turn may be used to understand the properties of these helices when present in bundles.

The methodology we have employed to generate M2 helices is one of simulated annealing via restrained molecular dynamics (SA/MD). This has the dual advantages of: (a) sampling a wide region of conformational space; and (b) producing an *ensemble* of final structures which is amenable to statistical analysis. The method is based on those employed to generate protein structures on the basis of internuclear separations derived from NMR experiments [18] and to refine X-ray diffraction based models [19]. We have investigated the effects of different treatments of electrostatic interactions during SA/MD on conformations of polar sidechains. We believe it is important to characterize the influence of electrostatic interactions on the conformations of functionally important polar sidechains eg. the EK (ie. Glu–Lys) pair which occurs near the N-terminus of the transmembrane M2-helix.

2. Methods

2.1. M2 sequences

M2 helices of δ and γ subunits of *Torpedo* nAChR have been generated using the SA/MD procedure. M2δ was selected to enable comparison with studies of the corresponding synthetic peptide [15]. M2γ was selected in order to allow comparison of the conformation of the EK (in M2δ) and QK (in M2γ) sidechain pairs at the N-termini of the helices. M2 helices were generated as running from E1′ (in M2δ) or Q1′ (in M2γ) to Q22′:

```
          1'                  11'                  22'
M2δ:-  Ac-E-K-M-S-T-A-I-S-V-L-L-A-Q-A-V-F-L-L-L-T-S-Q-NH2
M2γ:-  Ac-Q-K-C-T-L-S-I-S-V-L-L-A-Q-T-I-F-L-F-L-I-A-Q-NH2
```

(where the numbering scheme refers to the position within the M2 helix rather than within the parent protein). N-termini were blocked with an Ac group and C-termini with an amide so as to mimic preceding and following peptide bonds within the intact protein.

2.2. Simulated annealing / molecular dynamics

The SA/MD method used is similar to that of Nilges and Brünger [20], and was implemented using XPLOR version 3.1 [21] running on a Silicon Graphics R3000 Indigo. The CHARMM PARAM19 [22] parameter set was employed, with all H atoms explicitly included.

In *Stage 1* of SA/MD a Cα template was constructed by placing Cα atoms of an M2 sequence at their positions in an idealized α-helix. The remaining backbone and sidechain atoms were superimposed on the Cα atoms of the corresponding residues. These atoms 'grow out' from the Cα atoms, the positions of which remained fixed throughout *Stage 1*. Annealing started at 1000 K, during which weights for bond lengths and bond angles, and subsequently for planarity and chirality, were gradually increased. A repulsive van der Waals term was slowly introduced after an initial delay, the van der Waals radii being reduced to 90% of their standard values. Once the scale factors of these components of the empirical energy function reached their final values, the system was cooled from 1000 K to 300 K, in steps of 10 K and 0.5 ps. Electrostatic terms were *not* included during *Stage 1* and thus the

Table 1
Sidechain electrostatics

Simulation	Scaling of charges [a]	Dielectric model	Truncation [b]
I	$0.0 \rightarrow 0.0$	$\epsilon = r$	sw; $r_{ON} = 5$ Å; $r_{OFF} = 9$ Å
II	$0.05 \rightarrow 0.4$	$\epsilon = r$	sw; $r_{ON} = 5$ Å; $r_{OFF} = 9$ Å
III	$0.05 \rightarrow 1.0$	$\epsilon = r$	sw; $r_{ON} = 5$ Å; $r_{OFF} = 9$ Å
IV	$0.05 \rightarrow 1.0$	$\epsilon = 1$	sh; $r_{OFF} = 9.0$ Å

[a] Scale-factor applied to the partial atomic charges of polar sidechains during *Stage 2* of SA/MD.
[b] Method used to truncate electrostatic interactions between distant atom pairs during the same stage: sw = switch function; sh = shift function.
All other parameters are as defined in the Xplor 3.1 (Ref. [21]).

energy function was purely geometric in nature. Ten structures were generated for each M2 helix.

The resultant structures from *Stage 1* were each subjected to 5 molecular dynamics runs (*Stage 2*), resulting in an ensemble of 50 final structures. Initial velocities were assigned corresponding to 500 K. Harmonic restraints were imposed on Cα atoms at the beginning of *Stage 2*, and were gradually relaxed as the temperature was reduced from 500 to 300 K in steps of 50 K and 4 ps. On reaching 300 K, a 5 ps burst of constant temperature dynamics was performed, followed by 1000 steps of conjugate gradient energy minimization. During the latter burst of dynamics and energy minimization no restraints were imposed on the Cα atoms.

During *Stage 2* electrostatic interactions were introduced into the potential energy function. All mainchain atoms were assigned partial charges as defined by the PARAM19 parameter set. Partial charges on sidechain atoms of polar residues were gradually scaled up (see Table 1) as the temperature was reduced from 500 to 300 K. In order to mimic possible solvent screening of polar sidechain electrostatic interactions, four schemes for treatment of electrostatic interactions were introduced. As shown in Table 1, three classes of sidechain interactions were explored: (a) zero sidechain electrostatic interactions (simulation I) (b) screened interactions (simulations II and III) and (c) un-screened interactions (simulations IV). Simulations I, II and III differ in the scaling of partial charges of sidechains. Note that in each case the final scale factor for polar sidechain partial charges applied at the end of the 500 to 300 K cooling period was also used during the subsequent 5 ps burst of dynamics and during energy minimization. Each scheme (from I to IV) was applied for both M2δ and M2γ, resulting in 8 ensembles (M2δ-I, etc. and M2γ-I, etc.), each containing 50 structures, i.e. 400 structures in total.

The ensembles of structures thus generated were investigated with respect to their conformational properties. Root mean square deviations (RMSDs) from the average structure of an ensemble were determined separately for mainchain and sidechain atoms. Sidechain dihedral angles for polar residues were measured. Possible formation of ion pairs or H-bonds within N-terminal EK (in M2δ) or QK (in M2γ) pairs was evaluated. Conformational properties of EK and QK pairs from the high-resolution protein structures were obtained to aid our analysis of different simulations. The selection of protein structures from the PDB used in this study is described in the following section.

2.3. Selection of structures from the PDB

Proteins whose structures have been determined to a resolution of 2.0 Å or better were extracted from the Brookhaven Protein Data Bank (January 1992 release; [23]). All EK and QK sequence pairs were identified and side dihedral angles were evaluated. Dihedral angles χ_1, χ_2 of E/Q and χ_1, χ_2 and χ_3 of K have trimodal distributions, and may adopt one of the three preferred conformers: g^- ($+60°$), t ($180°$) and g^+ ($-60°$) ([24], definition of sidechain dihedral angles is according to IUPAC-IUB convention, 1970). Analysis of the stereochemical quality of protein structures suggests that very unusual χ's may signify a local error in a structure, even at 2.0 Å resolution [25]. Consequently, dihedrals which deviated from preferred conformers by more than $\pm 30°$ were flagged and the corresponding pairs were not considered for further analysis.

Among the high-resolution structures thus selected, there are many from the same or very similar proteins. To avoid bias, a list of *independent* sidechain pairs was compiled. A pair was defined as independent from another pair if: (i) the two pairs were from different proteins; (ii) the two pairs oc-

Table 2
EK and QK pairs selected from PDB

Protein name	PDB code	Chain	EK/QK pairs
Aldose A	1ALD		Q11, K12; Q85, K86; E206, K207; Q241, K242
Carbonic anhydrase	2CA2		Q158, K159
Chymotrypsin-alpha	5CHA	A	E78, K79
		B	Q81, K82
Chymotrypsinogen A	2CGA	A	E78, K79; Q81, K82
		B	E78, K79
Citrate synthase	1CTS		E299, K300
Cytochrome C	1CCR		E15, K16
Cytochrome C2	2C2C		E8, K9
Cytochrome C3	2CDV		Q44, K45
Cytochrome C peroxidase	2CYP		E267, K268
Cytochrome P 450	2CPP		Q343, K344
	3CPP		Q213, K214
Dihydrofolate reductase	8DFR		E62, K63; E126, K127; Q183, K184
Dihydrofolate reductase	4DFR	B	Q108, K109
Elastase	3EST		Q86, K87
Flavodoxin	3FXN		E13, K14
Flavodoxin	2FCR		E157, K158
Glutathione peroxidase	1GP1	A	E109, K110; E116, K117; E161, K162
Glutathione reductase	3GRS		E101, K102
Glycolate oxidase	1GOX		Q81, K82
Haemoglobin	2HHB	B	E7, K8
	1THB	D	Q131, K132
Haemoglobin V	2LHB		E135, K136
Immunoglobulin-FAB	2FB4	L	E205, K206
Immunoglobulin-lambda	2MCG	2	E207, K208
Interleukin-1-beta	1I1B		Q15, K16
	2I1B		E64, K65
Kallikrien A	2PKA	X	E23, K24
Lactate dehydrogenase	6LDH		Q324, K325
Lysozyme T4	1L01		E64, K65; Q123, K124
Myoglobin (sperm whale)	1MBD		E41, K42
	5MBN		E41, K42
	1MBW		E41, K42
Myoglobin (sea hare)	1MBA		E34, K35
Papain	9PAP		Q9, K10; E99, K100
Pea lectin	2LTN	C	E29, K30
Pseudoazurin	1PAZ		E116, K117
Plastocyanin	3PCY		E25, K26
Rat mast cell protease	3RP2	A	E38, K39; Q81, K82; E86, K87; E165, K166
		B	E109, K110
Ribonuclease A	1SRN	A	Q60, K61
	8RSA	B	Q60, K61
Superoxide dismutase	2SOD	O	E119, K120
Staphylococcal nuclease	1SNC		E52, K53
Thermolysin	1TMN	E	Q17, K18
Thymidilate synthase	2TSC	A	Q9, K10
Tonin	1TON		E166, K167
Trypsin beta	3PTN		Q221, K222
	2PTC	E	Q221, K222
	1TPA	E	Q221, K222
	1TGS	Z	Q221, K222
Trypsinogen-inhibitor	1TGS	I	Q51, K52
Ubiquitin	1UBQ		Q62, K63

curred at different positions within the same polypeptide chain; or (iii) the pairs belonged to different mutants/species/subunits of the same protein and differ in at least one of their sidechain dihedral angles (χ_1(E/Q), χ_2(E/Q), χ_1(K), χ_2(K)). The 67 independent pairs thus selected are listed in Table 2.

The possibility of forming an ion pair or H-bond was tested for each pair by measuring the distances between the end groups of E/Q and K sidechains.

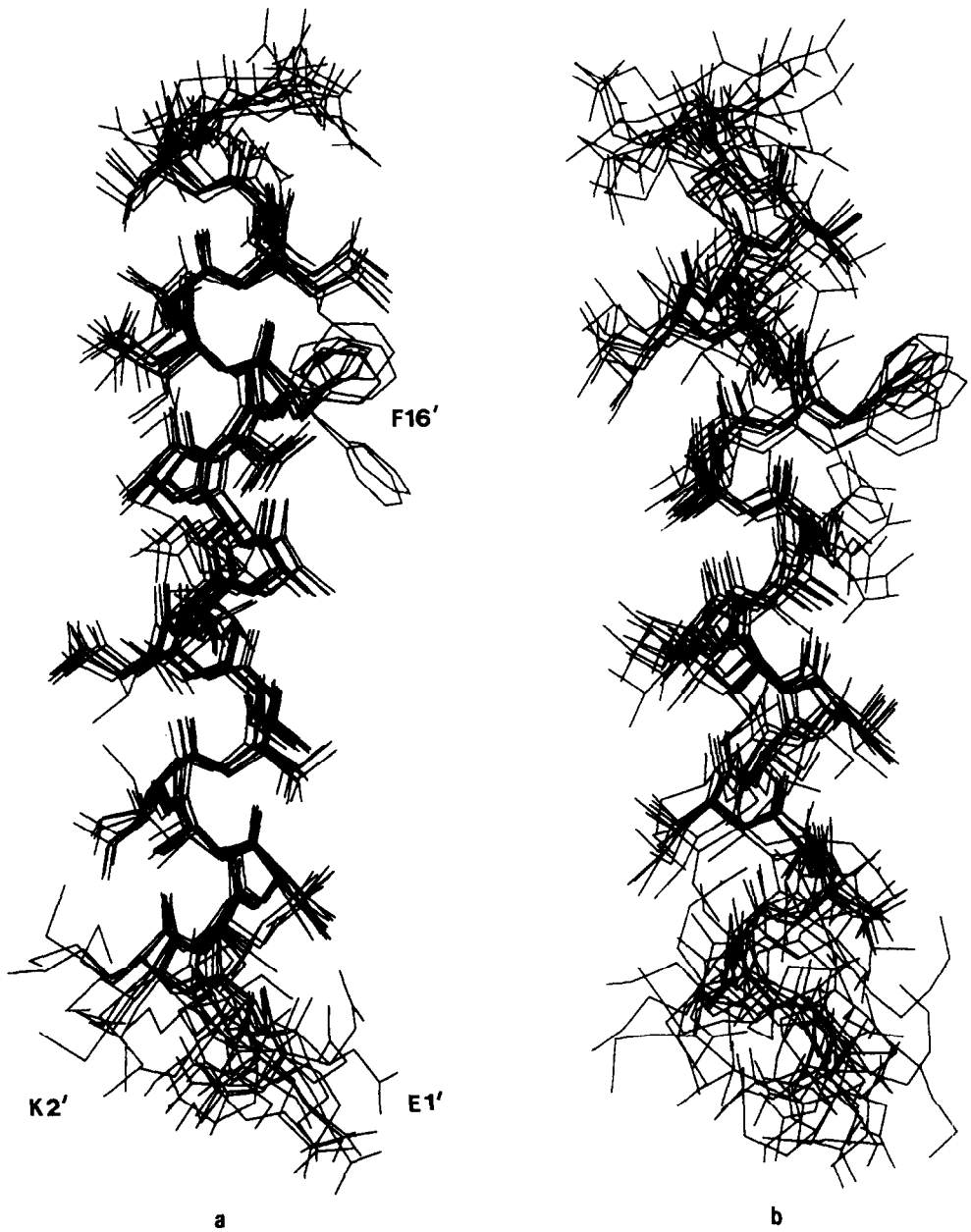

Fig. 1. Ten randomly selected SA/MD structures generated by simulations (a) M2δ-II and (b) M2δ-IV. Residues E1′ and K2′ (the N-terminal EK pair) and F16′ are indicated.

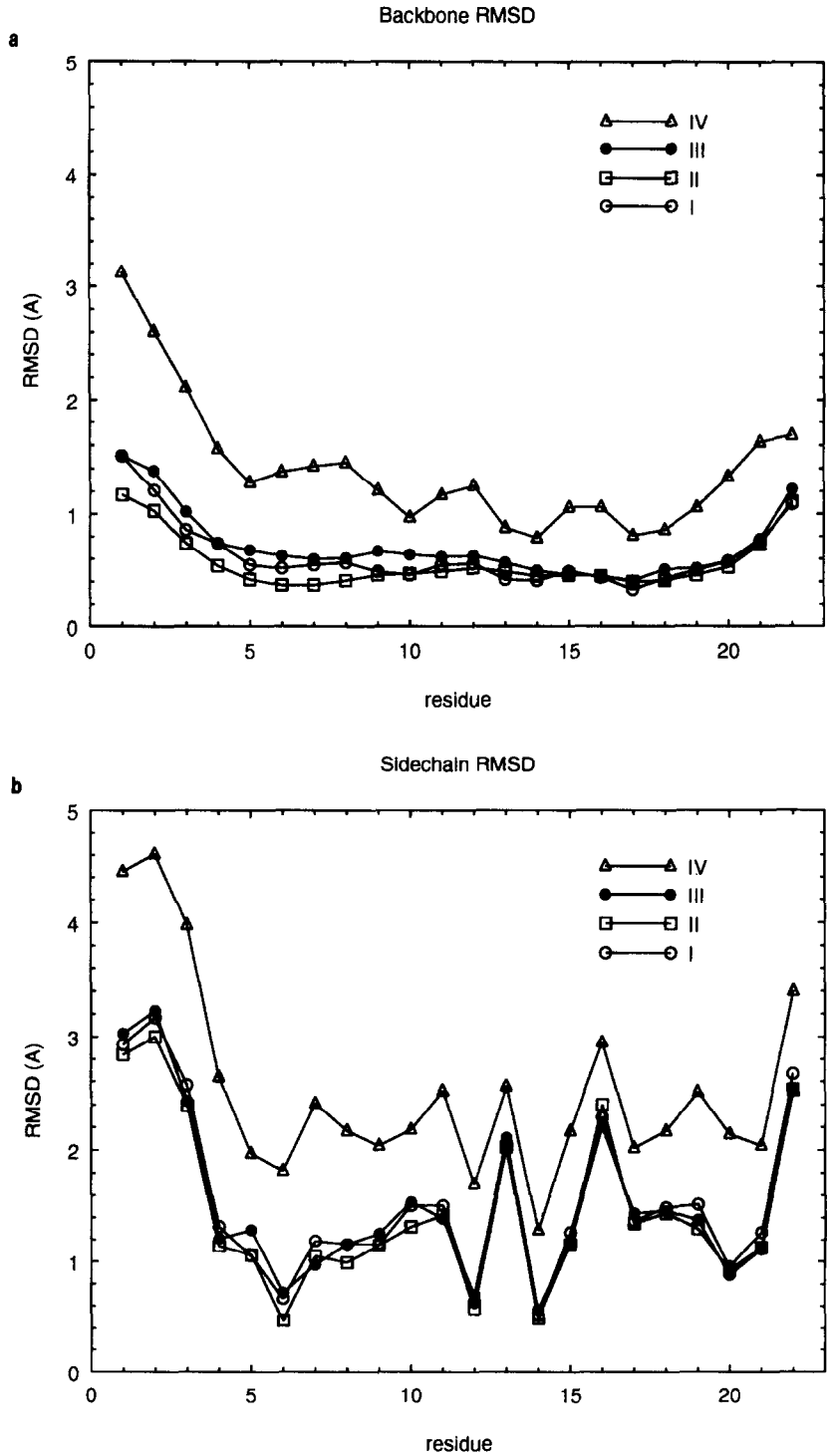

Fig. 2. RMSD vs. residue number for the four M2δ ensembles. RMSDs are shown for (a) mainchain atoms and (b) sidechain atoms

Table 3
RMSDs within ensembles

Ensemble	Mainchain RMSD (Å)	Sidechain RMSD (Å)
M2δ-I	0.74	1.82
M2δ-II	0.66	1.75
M2δ-III	0.80	1.82
M2δ-IV	1.50	2.77
M2γ-I	0.81	1.72
M2γ-II	0.64	1.63
M2γ-III	0.78	1.78
M2γ-IV	1.32	2.39

Atoms Oε1 and Oε2 of E, Oε1 and Nε2 of Q and Nζ of K were considered for this purpose. Pairs were also examined to determine whether they interact with other parts of the protein or crystallographically observed water molecules. Distances were calculated between the sidechains of the pairs and possible H-bonding groups from the rest of the protein and a cut-off of 4.0 Å was used.

3. Results

SA/MD generated ensembles of 50 M2δ and 50 M2γ structures for each of the four simulation conditions are defined in Table 1. Each ensemble of structures was analyzed as described in the Methods section.

3.1. RMSD between members of an ensemble

Analysis of RMSDs provides an overall estimate of the effect of different electrostatic models on variations in structure between different members of an ensemble. The results (Table 3) show that the overall backbone RMSD is lowest for simulations M2δ-II and M2γ-II (0.66 Å and 0.64 Å respectively). Corresponding RMSDs were somewhat higher (ca. 0.76 Å) in simulations I and III, and considerably higher (ca. 1.3 Å) in simulation IV. Overall, simulations which used a distance-dependent dielectric constant showed considerably smaller RMSDs than simulations with constant dielectrics. Such a difference has been observed in studies of myoglobin by Loncharich and Brooks [26] who found that simulations using a constant dielectric resulted in a larger RMSD, both from the average and the X-ray structures.

Ten randomly selected M2δ structures generated from simulations II and simulation IV (and thus exhibiting the smallest and the largest RMSDs re-

Table 4
Intra-helical H-bond distances in M2δ-ensembles

H-bond	M2δ-I	M2δ-II	M2δ-III	M2δ-IV
O1′...HN5′	2.11 (±0.62)	2.09 (±0.65)	2.21 (±0.68)	2.94 (±1.25)
O2′...HN6′	2.72 (±0.97)	2.48 (±0.88)	2.70 (±1.09)	3.73 (±1.63)
O3′...HN7′	2.19 (±0.81)	2.03 (±0.51)	2.24 (±0.82)	3.11 (±1.79)
O4′...HN8′	2.11 (±0.57)	1.96 (±0.41)	2.02 (±0.60)	2.41 (±0.76)
O5′...HN9′	1.92 (±0.25)	1.89 (±0.27)	2.02 (±0.51)	2.57 (±1.24)
O6′...HN10′	1.89 (±0.29)	1.86 (±0.03)	1.91 (±0.16)	2.39 (±0.87)
O7′...HN11′	**1.83 (±0.04)**	**1.83 (±0.03)**	**1.83 (±0.04)**	**1.99 (±0.33)**
O8′...HN12′	**1.86 (±0.05)**	**1.87 (±0.08)**	**1.84 (±0.04)**	**1.98 (±0.34)**
O9′...HN13′	**1.86 (±0.05)**	**1.86 (±0.07)**	**1.89 (±0.17)**	**2.08 (±0.38)**
O10′...HN14′	**1.83 (±0.04)**	**1.84 (±0.05)**	**1.87 (±0.08)**	**1.92 (±0.09)**
O11′...HN15′	**1.86 (±0.04)**	**1.87 (±0.06)**	**1.87 (±0.09)**	**1.93 (±0.08)**
O12′...HN16′	**1.88 (±0.13)**	**1.86 (±0.05)**	**1.85 (±0.05)**	**1.91 (±0.07)**
O13′...HN17′	**1.83 (±0.04)**	**1.83 (±0.04)**	**1.85 (±0.05)**	**1.94 (±0.13)**
O14′...HN18′	**1.85 (±0.05)**	**1.85 (±0.06)**	**1.85 (±0.05)**	**1.93 (±0.20)**
O15′...HN19′	**1.88 (±0.12)**	**1.85 (±0.12)**	**1.84 (±0.06)**	**1.92 (±0.16)**
O16′...HN20′	**1.84 (±0.05)**	**1.95 (±0.29)**	**1.91 (±0.12)**	**2.08 (±0.39)**
O17′...HN21′	1.92 (±0.18)	1.94 (±0.19)	2.01 (±0.27)	2.11 (±0.40)
O18′...HN22′	2.26 (±0.71)	2.07 (±0.61)	2.42 (±0.78)	2.92 (±0.93)
O19′...HN23′	2.19 (±0.66)	2.54 (±0.90)	2.21 (±0.73)	2.34 (±1.02)

Average H-bond distances (±SD) are listed in Å for the four M2δ ensembles. Those H-bonds which are conserved across all four simulations are shown in **bold**.

spectively) are shown in Fig. 1. The difference in backbone RMSDs is clearly visible. Furthermore, it is evident that even in ensemble M2δ-II there is variation in sidechain conformations, e.g. E1′, K2′ and F16′. Such variations are more marked in M2δ-IV. More detailed examination of RMSDs (Fig. 2a) reveals that, as anticipated, there is greater structural variation at the N- and C-termini. The overall pattern of variation of backbone RMSDs along the length of the helices are in accord with those seen in previous MD simulations of α-helices [27]. Sidechain RMSDs are low for residues 6′, 12′ and 14′, because these are alanine residues and hence show limited flexibility. Higher sidechain RMSDs are seen (Fig. 2b) for those residues, e.g. Q13′ and F16′, which are anticipated to adopt multiple conformations [28].

Intra-helical H-bonds formed between backbone carbonyl O and amide H atoms were also evaluated for each ensemble. Average H-bond distances between the ith carbonyl O and the $(i+4)$th amide H atoms for the M2δ models are given in Table 4. H-bonds near the N- and C-termini are somewhat longer, as observed in the protein crystal structures [29] and the standard deviations in H-bond length are high in these regions. Simulations IV in which $\epsilon = 1$, show longer H-bond distances (and larger standard deviations) even near the centre of the helix. We defined a H-bond as 'conserved' if, for each of the four ensembles, the mean O–H distance plus one SD was less than 3 Å. Those H-bonds which are conserved across all four simulations (indicated in **bold** in Table 4) are in the more hydrophobic C-terminal half of the helix (from O7′...HN11′ to O16′...HN20′). Similar results were obtained from the M2γ simulations (data not shown).

3.2. EK and QK pairs in M2 models

Dihedral angles χ_1 and χ_2 of residues E/Q1′ and K2′ were evaluated for all 400 structures from

Table 5
Distribution of EK and QK rotamers in M2δ-ensembles

EK pairs	M2δ-I	M2δ-II	M2δ-III	M2δ-VI	PDB [a]
(t t), (t t)	–	5.0	–	–	10.5
(t t), (g^+ t)	–	–	–	–	15.8
(g^+ t), (t t)	4.2	7.5	–	–	13.2
(g^+ t), (g^+ t)	8.3	2.5	–	–	10.5
(t t), (* *)	2.1	10.0	–	–	13.2
(g^+ t), (* *)	16.7	17.5	–	–	18.4
(* *), (t t)	22.9	22.5	3.3	–	2.6
(* *), (g^+ t)	12.5	17.5	30.0	22.2	5.3
(* *), (* *)	33.3	17.5	66.6	77.8	10.5
Total number of pairs	48	40	30	18	38
Q,K pairs	**M2γ-I**	**M2γ-II**	**M2γ-III**	**M2γ-IV**	**PDB [b]**
(t t), (t t)	6.4	2.3	2.4	–	6.9
(t t), (g^+ t)	10.6	2.3	2.4	2.8	–
(g^+ t), (t t)	–	4.6	2.4	2.8	13.8
(g^+ t), (g^+ t)	12.8	4.6	4.9	2.8	27.6
(t t), (* *)	4.2	4.6	7.3	2.8	6.9
(g^+ t), (* *)	8.5	6.9	7.3	2.8	20.7
(* *), (t t)	10.6	16.3	9.7	2.8	10.3
(* *), (g^+ t)	21.3	25.6	26.8	14.3	10.3
(* *), (* *)	25.5	32.6	36.6	68.6	3.4
Total number of pairs	47	43	41	35	29

The percentage of EK or QK pairs falling into each of the rotamer combinations is listed, where (* *) indicates a combination *other than* (t t) or (g^+ t).
[a] EK pairs. [b] QK pairs.

the M2 ensembles. Pairs whose χ_1 and χ_2 values fell within $\pm 30°$ of the preferred conformations, g^- ($+60°$), t ($180°$) and g^+ ($-60°$), were identified. These pairs were analyzed in further detail and compared with those selected from the PDB.

Sidechain dihedral angles

Results of analysis of sidechain dihedral angles of EK and QK pairs are summarized in Table 5. In order to determine whether the conformation of sidechain 1′ influences or is influenced by the conformation of sidechain 2′, dihedral angles χ_1(E/Q), χ_2(E/Q), χ_1(K) and χ_2(K) were grouped according to the corresponding combinations of rotamers. Thus, each dihedral angle may adopt one of three rotamers (g^-, t and g^+), and consequently there are 81 possible combinations of rotamers for the four dihedral angles. The frequency of occurrence of each combination was determined for all of the ensembles.

Simulation I (in the absence of any charges on the polar sidechains) provides an indication of the extent of randomization of sidechain conformations. Analysis of the rotamer combinations shows that 70 to 80% of EK and QK pairs occur either in (t t) or (g^+ t) in simulations I and II. Corresponding rotamer combinations for M2δ-III and M2δ-IV showed significant differences with only 22 (M2δ-IV) to 34% (M2δ-III) in (t t) or (g^+ t). Furthermore, the number of EK pairs which remain within $\pm 30°$ of the three preferred conformations is lower in simulations IV (in which $\epsilon = 1$). In general, the frequency of QK pairs which deviate from the preferred conformations is less than that of EK pairs. Furthermore, the percentage of QK pairs adopting (* *) (* *) conformations is significantly lower than that of EK pairs in simulation III.

Sidechain pairs in the PDB have a clear preference for certain rotamer combinations. The combinations (t t) (t t), (t t) (g^+ t), (g^+ t) (t t), (g^+ t) (g^+ t) together constitute about 50% of the total number of independent pairs. This is approximately the frequency expected on the basis of (χ_1, χ_2) frequencies for single sidechains, as estimated by McGregor et al. [24]. Overall, E/Q and/or K adopt (t t) or (g^+ t) conformations in ca. 90% of the independent pairs. Again, this was anticipated from single sidechain frequencies.

Interactions of the EK and QK pairs

Distances between the end groups of E(Q)1′ and K2′ sidechains were calculated in order to determine whether ion pairs and/or H-bonds were formed between the sidechains of a pair. The minimum distance between the end groups (d_1) was determined for each pair of an ensemble, and a cutoff of 3.5 Å was used to define a possible ion pair or H-bond in EK and QK pairs in the simulated and PDB structures.

The sidechain dihedral angles χ_1 and χ_2 deter-

Table 6
Analysis of approach of end-groups of sidechains ($d_1 < d_2$)

$d_1 < d_2$	Relative frequency (%)	Ion pairs or H-bonds (%)	d_1 (Å)	d_2 (Å)
M2δ-I	29.2	2.1	6.5 (±2.2)	7.2 (±1.9)
M2δ-II	32.5	17.5	4.6 (±2.1)	5.9 (±1.6)
M2δ-III	83.3	73.3	2.9 (±1.2)	4.8 (±1.2)
M2δ-IV	94.4	83.3	2.9 (±1.2)	4.7 (±0.9)
PDB[a]	26.3	0.0	6.3 (±1.4)	7.2 (±1.6)
M2γ-I	21.3	4.3	5.3 (±1.8)	6.4 (±1.5)
M2γ-II	27.9	11.6	4.6 (±1.8)	6.0 (±1.4)
M2γ-III	36.6	29.3	3.2 (±0.9)	4.8 (±0.6)
M2γ-IV	45.7	37.1	3.4 (±1.4)	5.5 (±1.1)
PDB[b]	13.8	0.0	6.4 (±1.6)	7.5 (±1.2)

Note that the mean values (±SD) of d_1 and d_2 refer to those sidechain pairs for which $d_1 < d_2$.
[a] EK pairs. [b] QK pairs.

mine the positions of sidechain atoms out to the Cδ atom. Residues E, Q and K have long sidechains and so have considerable flexibility beyond Cδ. Distances (d_2) between Cδ atoms of E/Q and K were computed for each pair, and were compared with the minimum distance between the end groups (d_1). When E/Q points towards K then $d_1 < d_2$. Conversely, when $d_1 > d_2$ then the sidechain of E/Q points away from that of K. Results of this analysis are presented in Table 6, and examples of EK pairs from the PDB in which $d_1 > d_2$ and in which $d_1 < d_2$ are shown in Fig. 3.

EK pairs from 10 randomly selected M2δ structures generated by simulations I to IV are shown in Fig. 4. Preliminary examination of these structures reveals that the end groups of the E and K sidechains approach one another more closely as one moves from simulation I to IV, i.e. as the degree of screening is reduced. Furthermore, the degree of formation of ion pairs increases, as is evident from the decrease in the mean value of d_1 in simulations III and IV (Table 6). The sharp increase in the number of EK pairs forming salt-bridges in simulations III is presumed to reflect the change in scaling of polar sidechain partial charges. The number of EK ion pairs was maximal in simulation M2δ-IV (83%) corresponding to the use of a constant dielectric.

QK pairs from 10 randomly selected M2γ structures generated by simulations I to IV are shown in Fig. 5. Examination of these structures reveals a much less marked change in sidechain conformations on going from M2γ-I to IV than was observed for the M2δ simulations. The number of QK pairs showing $d_1 < d_2$ increases only slightly as one moves from M2γ-I to M2γ-IV (from 21 to 46%). Furthermore, even in simulation IV only about 37% of QK

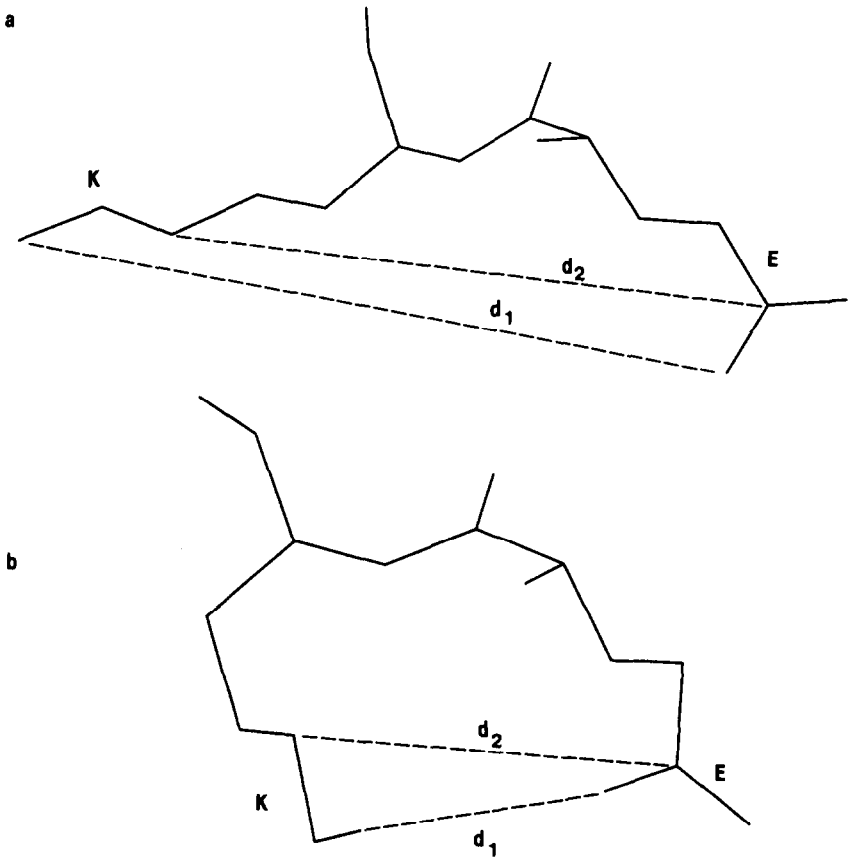

Fig. 3. Examples of EK pairs from the PDB: (a) from entry 2HHB for which $d_1 > d_2$ (d_1 = 11.86 Å; d_2 = 9.96 Å); and (b) from entry 1TON for which $d_1 < d_2$ (d_1 = 3.56 Å; d_2 = 5.08 Å). Both examples of EK pairs occur within α-helices.

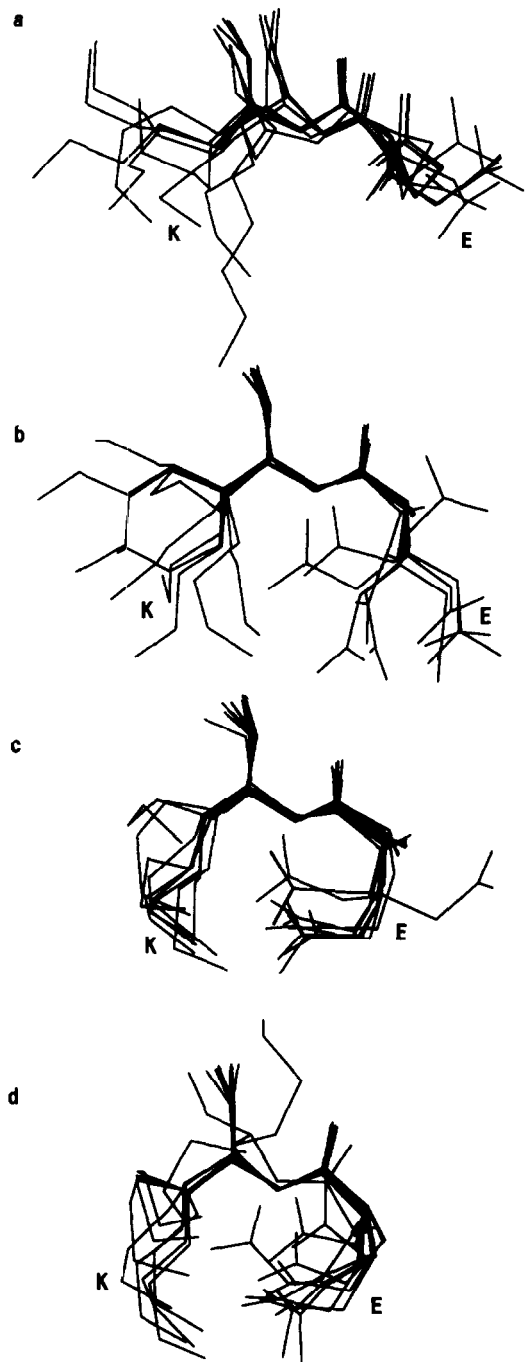

Fig. 4. EK pairs of 10 randomly selected structures from ensembles: (a) M2δ-I, (b) M2δ-II, (c) M2δ-III and (d) M2δ-IV. The pairs were superimposed for display using the mainchain atoms of residues 1′ and 2′.

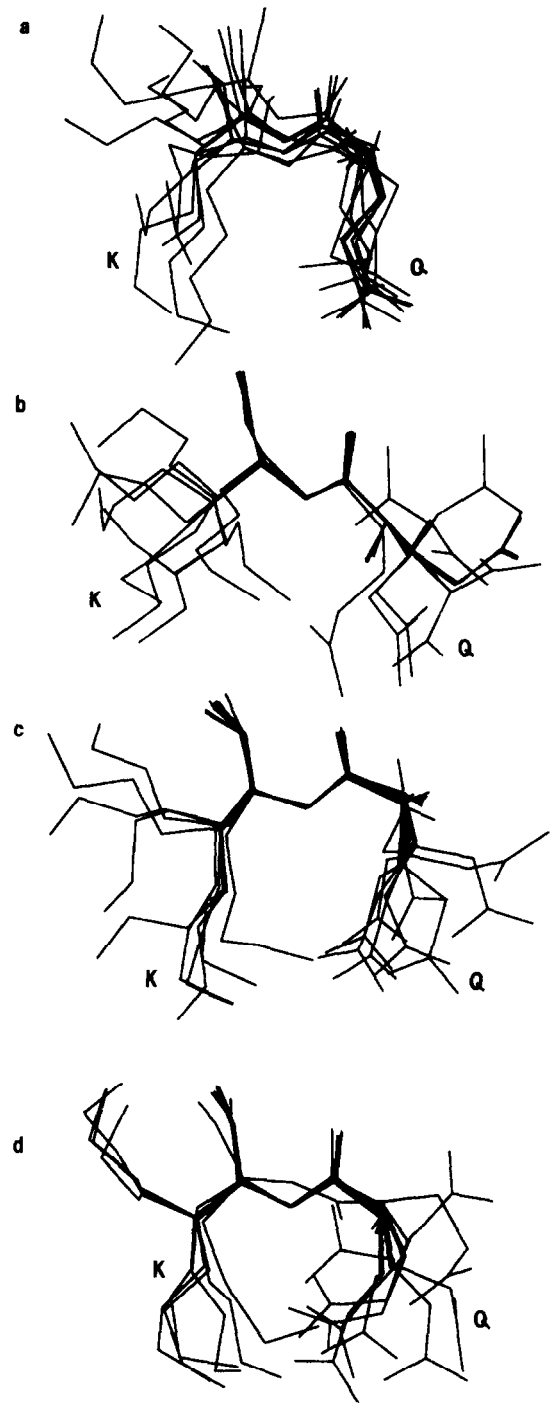

Fig. 5. QK pairs from 10 randomly selected M2γ structures from ensembles: (a) M2γ-I, (b) M2γ-II, (c) M2γ-III and (d) M2γ-IV. Other details as for Fig. 4.

pairs form H-bonds. This suggests that H-bond formation is less sensitive to the electrostatic model employed than is ion pair formation.

Distances between E, Q and K end groups and backbone nitrogen and carbonyl O atoms were determined for the M2 ensembles and for the selected sidechain pairs from the PDB. A cutoff of 3.0 Å (M2 models) or 3.5 Å (PDB) was used to define possible sidechain-mainchain interactions. The percentage of E1′ residues interacting with backbone nitrogen or carbonyl oxygen atoms vary between 35 and 50% between the four simulations. The situation is similar for Q sidechains in which about 35 to 65% of the Q′ residues interact with their own backbone atoms. An insignificant number of examples in which K2′ interacted with backbone carbonyl oxygen atoms was found amongst the K2′ sidechains in simulations I, II and III for both M2δ and M2γ helices. In contrast, e.g. M2γ-IV showed ca. 35% of K residues interacting with backbone carbonyl oxygens. Indeed, inspection of Fig. 5d suggests that the M2γ-IV structures fall into two distinct classes: (a) those in which K2′ interacts with the backbone carbonyl O of the same residue; and (b) those in which K2′ interacts with the sidechain of Q1′.

Table 7
Ser/Thr interactions in M2δ and M2γ ensembles

Residue	Ensemble	g^+	t	g^-
Ser-4′	M2δ-I	12 (2, 0)	23	15 (0, 5)
	M2δ-II	21 (3, 0)	24	5 (1, 4)
	M2δ-III	12 (5, 0)	27	10 (3, 5)
	M2δ-IV	12 (6, 1)	20	18 (1, 11)
Thr-5′	M2δ-I	39 (18, 0)	1	10 (8, 0)
	M2δ-II	31 (18, 0)	2	17 (14, 3)
	M2δ-III	32 (19, 0)	2	16 (9, 4)
	M2δ-IV	34 (12, 3)	1	15 (5, 1)
Ser-8′	M2δ-I	30 (17, 0)	15	5 (2, 0)
	M2δ-II	30 (28, 0)	13	7 (5, 5)
	M2δ-III	22 (19, 1)	22	6 (3, 5)
	M2δ-IV	27 (19, 0)	17	6 (1, 4)
Thr-4′	M2γ-I	47 (8, 0)	1	2 (2, 1)
	M2γ-II	42 (5, 1)	4	4 (2, 4)
	M2γ-III	45 (3, 0)	0	5 (1, 5)
	M2γ-IV	40 (0, 1)	0	10 (0, 4)
Ser-6′	M2γ-I	31 (15, 0)	15	4 (1, 1)
	M2γ-II	37 (33, 0)	10	3 (3, 1)
	M2γ-III	32 (26, 0)	12	6 (3, 4)
	M2γ-IV	31 (17, 1)	14	5 (1, 3)
Ser-8′	M2γ-I	25 (16, 0)	12	13 (3, 4)
	M2γ-II	22 (21, 0)	19	9 (5, 9)
	M2γ-III	25 (25, 0)	17	8 (4, 6)
	M2γ-IV	19 (18, 1)	23	8 (4, 4)

The figures in brackets indicate the number of serine/threonine residues interacting with the $i-4$ (first figure) and $i-3$ (second figure) carbonyl oxygens.

Analysis of E, Q and K interactions in conjunction with their sidechain conformations shows that when E/Q interacts with K or with its backbone atoms, the sidechain assumes (∗ ∗) (∗ ∗) or (∗ ∗) (g^+ t) conformations. Hence in simulations M2δ-III and -IV, in which ion pairs or backbone interactions are frequent, the percentage of EK pairs assuming (∗ ∗) (∗ ∗) and (∗ ∗) (g^+ t) conformations is also elevated.

Analysis of EK and QK pairs from the PDB shows that no salt-bridges or H-bonds are found in the pairs of selected structures. But in about 25% of EK pairs and 14% of QK pairs, the sidechains do approach one another (Table 6). Only about 4% of E/Q residues are found to interact with their own backbone nitrogen or carbonyl oxygen atoms. Distances between the end groups of the pairs and the potential hydrogen bonding groups from the rest of the proteins show that almost all pairs form salt-bridge or hydrogen bond either with the rest of the protein or with water molecules. This explains the increased percentage of extended conformations observed in the EK and QK pairs from the PDB structures relative to the simulated structures.

3.3. Serine and threonine conformations in M2 models

The conformations of serine and threonine residues in the M2 models are of interest for two reasons. Firstly, as discussed by Gray and Matthews [30], when present in α-helices, S and T residues have a propensity to adopt either a g^+ or g^- conformation, so as to enable H-bond formation to the carbonyl O of residue $i-3$ or $i-4$. On simple thermodynamic grounds this is expected to be particularly favoured for S/T residues in TM helices when located in a bilayer. Analysis of the conformations of these sidechains in simulated structures provides information how the different electrostatic models influence these sidechains. Moreover, the S

(or more rarely T) residues at positions 4′, 8′ and 12′ of M2 are of functional importance in that they line the central ion channel of nAChR. It has been suggested [31] that changes in the conformation of these residues may occur upon passage of an ion.

Values of χ_1 were evaluated for S/T residues at positions 4′, 5′ and 8′ of M2δ and positions 4′, 6′ and 8′ of M2γ (Table 7). Comparing S and T, it can be seen that T rarely occurred in a t conformation. This was as anticipated, because steric hindrance occurs between Cγ and O:i − 3 when T adopts this conformation whilst in an α-helix [30]. More detailed analysis of the results from all four simulations shows that S4′ in M2δ is more likely to adopt a t conformation. This is presumed to be because residue 4′ is in the first turn of the helix, and hence distortion of the N-terminus from the ideal helical conformation reduces the likelihood of $i-4$ H-bonds. The conformation of S6′ residue in M2γ models is predominantly g^+ as this residue has high propensity for H-bond formation to $i-4$ carbonyl oxygens. Though S8′ in both M2δ and M2γ shows a preference for g^+, significant numbers of them adopt t in all four simulations. This shows the inherent flexibility of this residue which may be of importance with respect to ion channel function.

Comparing simulations I to IV, for both M2δ and M2γ, no obvious trends are evident. Interestingly, despite the higher N-terminal RMSDs of simulations IV, there is no increase in the frequency of the t conformation for residue 4′. There is, however, a small increase in the frequency of the g^- conformation for this residue. This suggests that deviations for helical backbone geometry may be correlated with an increase in g^- $(i-3)$ H-bonding. However, the overall similarity between the four simulations suggests that, as anticipated, the conformations of the less flexible polar sidechains do not seem to be greatly influenced by the electrostatic model employed.

4. Discussion

4.1. SA / MD and M2-helix models

An advantage of SA/MD is that it produces an *ensemble* of structures, statistical analysis of which provides estimates of the relative probabilities of different sidechain conformations, subject to restraints employed in generating the model. As mentioned earlier, this method is derived from techniques used to determine molecular structures on the basis of NMR data [32] and also used to refine X-ray diffraction derived models [19]. A similar method has been used to predict the conformation of the dimerization domain of the GCN4 leucine zipper [20] in advance of the X-ray structure, and more recently has been employed to model dimerization of glycophorin transmembrane helices [33]. An analogous method has been used by Laughton [34], in the context of homology modelling, to generate amino acid sidechain conformations. We have employed SA/MD to model bundles of parallel transmembrane helices as found in certain ion channels [35]. Overall, studies both by us and by other investigators demonstrate that this method will generate structural features not explicitly included in the initial Cα template.

Molecular dynamics (MD) simulations comparing distance-dependent and constant dielectric models have been carried out on globular proteins such as myoglobin [26], the *Trp* repressor [36], and lysozyme [37]. MD simulations with a constant dielectric generally show large RMSD values from average and X-ray structures. Our results on M2 models using SA/MD procedure strengthen this conclusion. Simulations using a constant dielectric (IV) resulted in large RMSDs from the average of the ensemble, whereas simulations using distance-dependent dielectrics (I to III) resulted in significantly smaller RMSD values.

Comparison of results from simulations I to IV allows analysis of the effects of varying the different components of the electrostatic models. Simulation I was carried out mainly to indicate the randomization of sidechain conformations in the absence of electrostatic interactions. Comparison of simulations II and III enables one to assess the effects of scaling of polar sidechain partial charges (Table 1). There is little difference between the mainchain conformations of II and III, as judged by both mainchain RMSDs and H-bond lengths. However, the EK (and to a lesser extent the QK) rotamer distributions and the degree of ion pair formation in III differ somewhat from those in II. This suggest that scaling of

polar sidechain partial charges may be necessary to prevent overestimation of interactions in isolated TM helices. The most dramatic changes are seen for simulations IV in which a constant dielectric was employed. The simulations show changes in the backbone geometry relative to the other three simulations. If one considers the central 10 residues of M2, the mainchain RMSD is increased from ca. 0.5 Å for simulations I to III to ca. 1 Å for IV. For the same residues, the mainchain H-bond length increases from ca. 1.9 to ca. 2.1 Å. Thus, in the absence of additional terms to maintain backbone H-bonds, use of a constant dielectric results some distortion loosening of α-helices. Even more evident is the change in EK and QK interactions. The use of a constant dielectric leads to considerable overestimation of the frequency of ion pair (and to a lesser extent in M2γ H-bond) interactions between polar sidechains. The pattern of intra-helical H-bonds in the C-terminal half of M2 is conserved in all four simulations, mainly due to the absence of competing polar sidechains from this region.

4.2. Possible implications with respect to nAChR function

Several theoretical studies have been reported on the importance of EK pairs in nAChR function [38]. For example, Furois-Corbin and Pullman investigated models of pentameric bundles of nAChR M2 helices [39–41]. Energy minimization studies on model α-helices containing EK or QK pairs indicated that the lowest energy conformation contained a strong ion pair/H-bond between the sidechains of E/Q and of K. Hence, in their calculations on M2 helix bundles it was assumed that the sidechains of E/Q1′ and K2′ form such intra-helix interactions. Subsequent calculations of the potential energy of an ion passing through the channel suggested that the EK pair at the N-terminus of M2 facilitates entry/exit of cations to/from the channel.

In the present studies, simulations were carried out in vacuo on isolated M2 helices employing different dielectric models. Analysis of the simulated structures shows the extent of EK conformations depending upon the electrostatic interactions. Low dielectric ($\epsilon = 1$) simulations resulted in markedly enhanced formation of ion pairs and sidechain/main-chain and sidechain/sidechain interactions for polar residues over those observed for the $\epsilon = r$ dielectric models for isolated helices.

EK pairs from the PDB structures show properties which are somewhat different from simulations II and significantly different from simulations III and IV. The difference in EK conformations in globular proteins is due to the predominant interactions of both E and K residues with the water molecules and other parts of the protein. The EK pairs in the nAChRs are present in an environment different from those represented within the PDB. In intact nAChR, EK pairs are thought to lie at the mouth of the channel. In the M2 peptide, which appears to span the lipid bilayer, they will lie close to the water/bilayer interface. MD simulations [42] and combined X-ray/neutron diffraction studies [43,44] on lipid bilayers suggest that there is some penetration of water molecules into the lipid region, close to membrane–water interface. The dielectric constant in the interface region may be expected to be somewhere between that of an alkane ($\epsilon = 2$) and water ($\epsilon = 80$).

Within intact nAChR, glutamate (E1′) and glutamine (Q1′) residues form a functionally important 'intermediate ring' of sidechains which is believed to constitute the narrowest part of the open channel [45,46]. Therefore, the interactions of these sidechains will affect ion transport through the pore and so attempts to understand such interactions assume significance. Previous theoretical studies [39] on nAChR channels assumed a salt-bridge (or H-bond) between the sidechains of E1′ (or Q1′) and K2′. In contrast the current study has demonstrated the sensitivity of E1′ (and K2′) sidechain interactions to the treatment of electrostatic interactions. This is especially important, given the location of these residues close to the membrane–water interface (see above) and in the light of very limited experimental data concerning their conformations.

It is still not clear whether E1′ residues interact directly with permeant ions or merely contribute to the overall electrostatic field. As observed in the present studies, a change in the screening of E1′ sidechain electrostatic interactions is coupled to changes in the conformations of these sidechains. An extension of our studies to M2 pentameric helix bundles suggests that altering the electrostatic model

can change E1′ orientations with respect to the pore, resulting in a variation in the pore radius (unpublished results). Thus the orientation of E1′ sidechains is of *functional* importance. To complicate matters further, Hucho and Hilgenfeld suggest that upon ion transfer through the channel, the E1′ sidechains may undergo conformational changes [47]. Furthermore, local pK_A values of E1′ should be considered when studying pentameric bundles of M2 helices. In the context of these numerous factors, it is essential that we fully comprehend the nature of electrostatic interactions both within and between M2 helices. This is only possible if one proceeds in a step-by-step manner. We are currently investigating the effect of different electrostatic models on the structural properties of M2 helix bundles.

Acknowledgements

This work was supported by a grant from the Wellcome Trust. Our thanks to Ian Kerr and Jason Breed for discussions, and to the Oxford Centre for Molecular Sciences for provision of computational facilities.

References

[1] J.L. Popot, Curr. Opin. Struct. Biol., 3 (1993) 532.
[2] K.V. Pervushin and A.S. Arseniev, FEBS Lett., 308 (1992) 190.
[3] A.L. Lomize, K.V. Pervushin and A.S. Arseniev, J. Biomol. NMR, 2 (1992) 361.
[4] M.S.P. Sansom, Prog. Biophys. Mol. Biol., 55 (1991) 139.
[5] J.P. Changeux, J.l. Galzi, A. Devillers-Thiéry and D. Bertrand, Q. Rev. Biophys., 25 (1992) 395.
[6] C. Toyoshima and N. Unwin, Nature, 336 (1988) 247.
[7] N. Unwin, J. Mol. Biol., 230 (1993) 1101.
[8] J. Giraudat, M. Dennis, T. Heidmann, P.Y. Haumont, F. Lederer and J.P. Changeux, Biochemistry, 26 (1987) 2410.
[9] F. Hucho, W. Oberthür and F. Lottspeich, FEBS Lett., 205 (1986) 137.
[10] K. Imoto, C. Busch, B. Sakmann, M. Mishina, T. Konno, J. Nakai, H. Bujo, Y. Mori, K. Fukuda and S. Numa, Nature, 335 (1988) 645.
[11] R.J. Leonard, C.G. Labarca, P. Charnet, N. Davidson and H.A. Lester, Science, 242 (1988) 1578.
[12] P. Charnet, C. Labarca, R.J. Leonard, N.J. Vogelaar, L. Czyzyk, A. Gouin, N. Davidson and H.A. Lester, Neuron, 2 (1990) 87–95.
[13] F. Revah, D. Bertrand, J.L. Galzi, A. Devillers-Thiery, C. Mulle, N. Hussy, S. Bertrand, M. Ballivet and J.P. Changeux, Nature, 353 (1991) 846.
[14] M.S.P. Sansom, Curr. Biol., 3 (1993) 239.
[15] S. Oiki, W. Danho, V. Madison and M. Montal, Proc. Natl. Acad. Sci. USA, 85 (1988) 8703.
[16] S. Oiki, V. Madison and M. Montal, Proteins: Struct. Func. Genetics, 8 (1990) 226.
[17] B. Bechinger, Y. Kim, L.E. Chirlian, J. Gesell, J.-M. Neumann, M. Montal, J. Tomich, M. Zasloff and S.J. Opella, J. Biomol. NMR, 1 (1991) 167.
[18] A.T. Brünger and M. Karplus, Acc. Chem. Res., 24 (1991) 54.
[19] A.T. Brünger, A. Krukowski and J.W. Erickson, Acta Cryst., A46 (1990) 585.
[20] M. Nilges and A.T. Brünger, Prot. Eng., 4 (1991) 649.
[21] A.T. Brünger, X-PLOR, Version 3.0, Yale University Press, New Haven, CT, 1992.
[22] B. Brooks, R. Bruccoleri, B. Olafson, D. States, S. Swaminathan and M. Karplus, J. Comp. Chem., 4 (1983) 187.
[23] F. Bernstein, T. Koetzle, G. Williams, E. Meyer, M. Brice, J. Rodgers, O. Kennard, T. Shimanouchi and M. Tasumi, J. Mol. Biol., 112 (1977) 535.
[24] M.J. McGregor, S.A. Islam and M.J.E. Sternberg, J. Mol. Biol., 198 (1987) 295.
[25] A.L. Morris, M.W. MacArthur, E.G. Hutchinson and J.M. Thornton, Proteins: Struct. Func. Genetics, 12 (1992) 345.
[26] R.J. Loncharich and B.R. Brooks, Proteins: Struct. Func. Genetics, 6 (1989) 32.
[27] R.M. Levy, D. Perahia and M. Karplus, Proc. Natl. Acad. Sci. USA, 79 (1982) 1346.
[28] C.L. Brooks, M. Karplus and B.M. Pettitt, in Proteins: a Theoretical Perspective of Dynamics, Structure and Thermodynamics, Wiley, New York, 1988.
[29] E.N. Baker and R.E. Hubbard, Prog. Biophys. Mol. Biol., 44 (1984) 97.
[30] T.M. Gray and B.M. Matthews J. Mol. Biol., 175 (1984) 75.
[31] M.S.P. Sansom, Eur. Biophys. J., 21 (1992) 281.
[32] M. Nilges, M.C. Clore and A.M. Gronenborn, FEBS Lett., 239 (1988) 129.
[33] H.R. Treutlein, M.A. Lemmon, D.M. Engelman and A.T. Brünger, Biochemistry, 31 (1993) 12726.
[34] C.A. Laughton, Prot. Eng., 7 (1994) 235.
[35] I.D. Kerr, R. Sankararamakrishnan, O.S. Smart and M.S.P. Sansom, Biophys. J., 67 (1994) 1501.
[36] J. Guenot and P.A. Kollman, Protein Sci., 1 (1992) 1185.
[37] G.E. Arnold and R.L. Ornstein, Proteins: Struct. Func. Genetics, 18 (1994) 19.
[38] G. Eisenman and O. Alvarez, J. Membrane Biol., 119 (1991) 109.
[39] S. Furois-Corbin, and A. Pullman, Biochim. Biophys. Acta, 984 (1989) 339.
[40] S. Furois-Corbin and A. Pullman, FEBS Lett., 252 (1989) 63.

[41] S. Furois-Corbin and A. Pullman, Biophys. Chem., 39 (1991) 153.
[42] E. Egbert, S.-J. Marrink and H.J.C. Berendsen, Eur. Biophys. J., 22 (1994) 423.
[43] G. Büldt, H.U. Gally and J. Seelig, J. Mol. Biol., 134 (1979) 673.
[44] G. Zaccai, J.K. Blasie and B.P. Schoenborn, Proc. Natl. Acad. Sci. USA, 72 (1980) 376.
[45] K. Imoto, FEBS Lett., 325 (1993) 100.
[46] N. Unwin, Nature, 373 (1995) 37.
[47] F. Hucho and R. Hilgenfeld, FEBS Lett., 257 (1989) 17.